Microporous Ni-Doped TiO_2 film Photocatalyst by Plasma Electrolytic Oxidation

Zhongping Yao,*,† Fangzhou Jia,† Shujun Tian,† ChunXiang Li,† Zhaohua Jiang,† and Xuefeng Bai‡

School of Chemical Engineering and Technology, Harbin Institute of Technology, No. 92 Xidazhijie Street, Nangang, Harbin 150001, P.R. China, and Heilongjiang Institute of Petrochemistry, Harbin 150040, P.R. China

ABSTRACT Ni-doped TiO_2 film catalysts were prepared by a plasma electrolytic oxidation (PEO) method and were mainly characterized by means of SEM, EDS, XRD, XPS, and DRS, respectively. The effects of Ni doping on the structure, composition and optical absorption property of the film catalysts were investigated along with their inherent relationships. The results show that the film catalyst is composed of anatase and rutile TiO_2 with microporous structure. Doping Ni changes the phase composition and the lattice parameters (interplanar crystal spacing and cell volume) of the films. The optical absorption range of TiO_2 film gradually expands and shifts to the red with increasing dosages. Both direct and indirect transition band gaps of the TiO_2 films are deduced consequently. Moreover, the photocatalytic activity of the film catalysts for splitting $Na_2S+Na_2SO_3$ solution into H_2 is enhanced by doping with an appropriate amount of Ni. The as-prepared TiO_2 film catalyst doping with 10 g/L of $Ni(Ac)_2$ presents the highest photocatalytic reducing activity.

KEYWORDS: TiO_2/Ti film catalyst • Ni-doping • Plasma electrolytic oxidation • H_2 evolution

1. INTRODUCTION

There has been great interest in titania (TiO_2) because of its chemical stability, photocatalytic activity and wide applications in many fields (1). In the field of photocatalysis, polycrystalline titania doped by transition metal-ion (such as V (2), Cr (3, 4), Fe (5), Co (6), Ni (7), Mn (8), Mo (2), Cu (9), and Zn (10)) has been one of the most important research areas all the times. Generally compared with undoped TiO_2, the transition metal-ion doped TiO_2 usually has a smaller grain size, a larger specific surface area and a narrower band gap, and its absorption edge shifts to the red. And most of the doped transition metal ions are considered to inhibit the phase transformation from anatase to rutile. Among all kinds of preparation methods of the doped TiO_2 catalysts, the sol−gel method is most widely used by many researchers (1, 7−9). Also, some other methods such as solvothermal method (4), flame spray synthesis (4), Rf-magnetron sputtering (2), liquid phase deposition (11), establish and develop gradually as well.

Plasma electrolytic oxidation (PEO), also called micro arc oxidation, can be used to prepare TiO_2 film photo catalyst on Ti alloys. Since X. Z. Li, et al. (12) for the first time reported the preparation of Ti/TiO_2 mesh electrode by spark anodizing Ti mesh in 0.5 M H_2SO_4 solution in 2000, this method attracts much attention in the world because such kind of film catalysts present high catalytic activity and a large surface area and micro porous surface structure. Han et al. (13) prepared nanocrystallized SrHA/SrHA−$SrTiO_3$/$SrTiO_3$−TiO_2 multilayer coatings and discussed the photocatalytic application. Wan et al. (14) prepared a series of Cr-doped TiO_2 film catalysts in $Na_3PO_4+K_2Cr_2O_7$ solution, which showed an excellent photocatalytic effect for degradation of methylene blue and decomposition of water under visible light illumination. Our group (15) prepared Zn-doped TiO_2 film catalysts and investigated the photocatalytic reductive property in the potassium chromate solution. Besides, Bayati et al. (16−18) prepared vanadia−titania composite layers with micro/nanoporous structure, investigated the photocatalytic property through the degradation of methylene blue and found that the composite layers exhibited a significantly enhanced photoactivity when compared to pure TiO_2 layer without doping.

Among the different transition metal ion dopants, low-valence Ni^{2+} doping is generally considered to improve the photoactivity of titania in many references (19−21). However, Ni-doped TiO_2 film catalysts by PEO method are seldom reported. In this work, the Ni-doped TiO_2/Ti film photo catalyst was prepared on TA1 in the phosphate solution mixed with $Ni(Ac)_2$, the structure, composition, and optical absorption property were investigated and at the same time the photocatalytic splitting $Na_2S+Na_2SO_3$ solution in H_2 was carried out to evaluate the photocatalytic property.

2. MATERIALS AND METHODS

2.1. Preparation of Film Catalysts. A piece of raw Ti plate (purity >99.6%) with the dimension of 18 cm^2 was used as working electrode and the electrolyzer made of stainless steel served as the counter electrode. A homemade pulsed-single polar PEO electrical source with power of 5 kW was used in PEO process for 10 min. The electrolyte solution contained KOH (7 g/L), $(NaPO_3)_6$ (10 g/L), and $Ni(Ac)_2$ (0−20 g/L). The working frequency was 2000 Hz and the peak current density was 2 A/cm^2. The reaction temperature was controlled to be below 30 °C by adjusting the cooling water flow. After the treatment,

* Corresponding author.
Received for review May 20, 2010 and accepted August 20, 2010
† Harbin Institute of Technology.
‡ Heilongjiang Institute of Petrochemistry.
DOI: 10.1021/am100450h

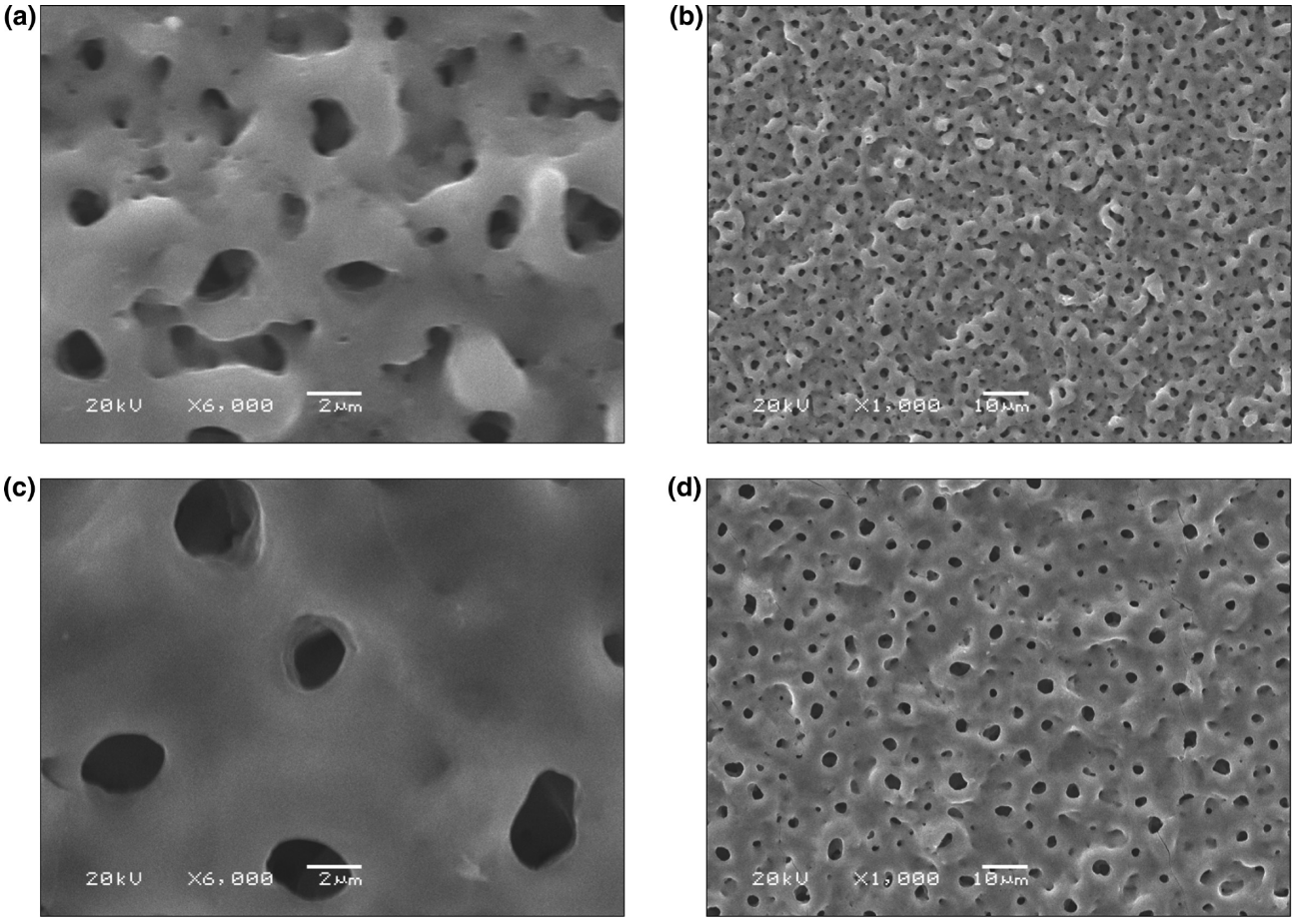

FIGURE 1. Surface SEM of the film catalysts prepared with and without doping: (a, b) 0 g/L; (c, d) 10 g/L $Ni(Ac)_2$.

the films were flushed with water and dried in air. Deionized water was used in all experiments.

2.2. Characterization of Film Catalysts. Morphology images of the film catalysts were studied with scanning electron microscopy (SEM, JSM-6480A, Japan). The relative contents of elements in the film catalyst were investigated by energy dispersive spectroscopy (EDS, JED-2200, Japan). Phase composition was examined with X-ray diffraction (XRD, D/max-rB, Ricoh, Japan), with a Cu Ka source. The film was analyzed by X-ray photoelectron spectroscopy (XPS) to investigate the surface composition and the valence state (Phi5700 ESCA system, U.S.A.) The binding energies were calibrated with respect to the signal for adventitious carbon (binding energy, 284.6 eV). The UV−vis DRS spectra of the samples were recorded with a UV−vis spectrophotometer (UV-2400, Shimadzu, Japan).

2.3. Photocatalytic Splitting Na_2S+Na_2SO_3 Solution into H_2. The photo catalytic experiments were carried out in a 100 mL annular quartz photochemical reactor with 100 mL Na_2S+Na_2SO_3 aqueous solution placed in vertical position which was illuminated by an external-side UV-A high-pressure mercury lamp (125W) placed in fixed position. The initial concentrations of Na_2S and Na_2SO_3 were 0.10 and 0.02 mol/L, respectively. The solution was continuously stirred with a magnetic stirrer. The film catalyst (surface area 9 cm^2) was placed in the middle of the reactor, and the distance between the lamp and the film catalyst was 4 cm. Prior to irradiation, the solution was purged with nitrogen for half an hour, which also ensured the sufficient adsorption equilibrium on the surface of the catalyst. The amount of H_2 at different times was measured as the sole gaseous substance via gas chromatographic analysis (SP2100A, Beifen instrument, China).

3. RESULTS AND DISCUSSION

3.1. Microporous Structure of Film Catalysts. The film catalysts prepared under different dosages of $Ni(Ac)_2$ are of different colors, with a thickness of 1 μm or so. The film without doping is blue gray. After doping, the film turns into yellow green, which is deeper and darker with the increase in the dosage. Figure 1 is the surface SEM of the film catalysts, which shows that many microholes are distributing almost evenly on the surface. The big microholes are about a few micrometers, whereas the small microholes are less than a micrometer, which presents that the films are of micro porous structure. With the increase in the dosage, the size of the micropores is increased while the number of the micropores is decreased.

3.2. Phase Composition and Lattice Parameters of Film Catalysts. As widely known, the color of Ni^{2+} ion is generally green, which corresponds with the colors of film, which illustrates that the Ni comes into the film. To verify this, we fulfilled the EDS and XRD analyses. Table 1 is the relative contents of the main elements in the films by EDS analysis. It can be noted from Table 1 that the film is mainly composed of O, Ti, and P. Ti and P contents are increased while O content is almost unchanged with the dosage. Meantime, Ni also exists in the film after doping and its amount is increased with the dosage.

Table 1. Relative Contents of the Main Elements in Film Catalysts Prepared with Different Dosages of $Ni(Ac)_2$ by EDS Analysis

	at %			
	0 g/L	1 g/L	5 g/L	10 g/L
O	76.52	75.21	76.94	75.25
P	2.33	2.99	3.26	4.75
Ti	20.93	21.24	18.36	16.93
Ni	0	0.22	1.07	2.45

Figure 2a is the XRD patterns of the films prepared with different dosages. TiO_2 exists in two main crystallographic forms (anatase and rutile) in the films. The diffraction peaks corresponding to the substrate emerges in the film due to the porosity and very small thickness of the film. Increasing the dosage of $Ni(Ac)_2$, the amount of anatase is increased and then decreased gradually, whereas the amount of rutile is decreased and then increased gradually according to the relative intensity of characteristic peaks. By comparison, it can be confirmed that doping Ni promotes the crystallization of anatase and inhibits the phase transformation from anatase to rutile as well (when the dosage is less), and then when the dosage is more, the doping Ni promotes the phase transformation from anatase to rutile. Contrary to the EDS results, XRD analysis does not show any diffraction peaks corresponding to the substances containing Ni, and therefore, Ni maybe exists in the form of amorphous state in the films.

Panels b and c in Figure 2 show the changes of 2θ corresponding to the anatase (101) and rutile(110) with the increase of the dosage. According to Bragg's eq $2d\sin\theta = \lambda$, the change of theta influences the value of d, which indicates that the interplanar crystal spacing is changed by the dosage. Table 2 is the lattice parameters of TiO_2 in the film calculated through jade software 5.0. Both the interplanar crystal spacing and the cell volume show the similar changing regularity: with the increase of dosage, the interplanar crystal spacing and the cell volume first decrease, then increase and finally decrease again. The film doped with 10 g/L $Ni(Ac)_2$ has the similar values of the lattice parameters to that undoped. The above results may be generally determined by two reverse effects, i.e., the stress of the film and the amount of the doping substance. The compressive stress is generally formed due to the growth of oxide film because the oxide usually has a larger volume than that of the metal substrate (22), which is liable to result into the decrease of the cell volume and the interplanar crystal spacing of TiO_2. On the other hand, the radius of Ni^{2+} is 69 pm and larger than that of Ti^{4+} (60.5 pm), which means that if the Ni^{2+} comes into the lattice of TiO_2, the cell volume and the interplanar crystal spacing will be expanded. When the former effect is stronger than the latter (i.e., the dosage is 1 g/L), the cell volume and the interplanar crystal spacing are reduced. With the increase in dosage, when the latter effect is gradually stronger than the former, the expanding of the cell volume and the interplanar crystal spacing is increased. However, the limited solubility of amount of Ni^{2+} in the lattice of TiO_2 indicates the expanding effect is also limited,

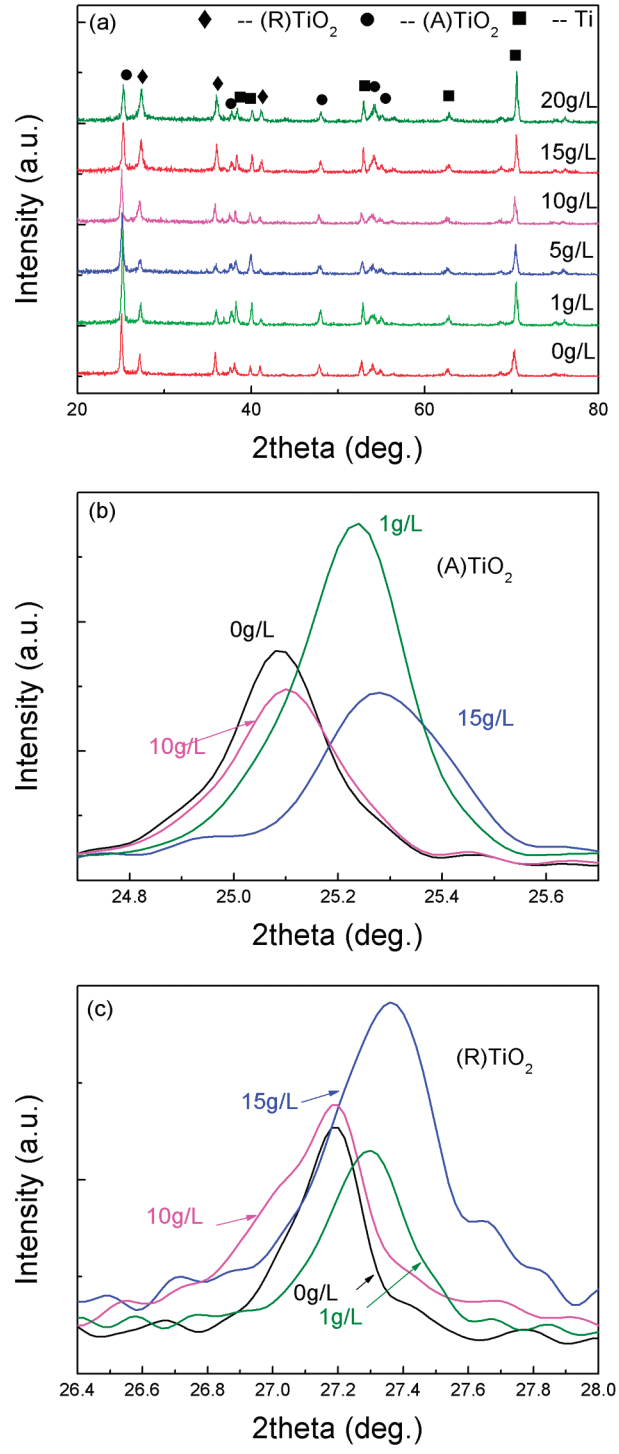

FIGURE 2. (a) XRD patterns of film catalysts prepared with different dosages; (b) enlarged picture of the anatase TiO_2 (101); (c) enlarged picture of the rutile TiO_2(110).

whereas the stress effect still exists with the doping; therefore, the cell volume and the interplanar crystal spacing are decreased again with the further increase in dosage.

3.3. XPS Analysis of Film Catalysts. The XPS spectra of Ti_{2p}, Ni_{2p}, and O_{1s} of undoped and doped TiO_2 $Ni(Ac)_2$ were investigated, with the results shown in Figure 3. Panels a and b in Figure 3 show the XPS peaks of $Ti_{2p}1/2$, $Ti_{2p}3/2$, $Ni_{2p}1/2$ and $Ni_{2p}3/2$, are symmetrical, and the XPS peak positions of $Ti_{2p}1/2$, and Ti_{2p} 3/2 $Ni_{2p}1/2$, and $Ni_{2p}3/2$

Table 2. Lattice Parameters of Film Catalysts Prepared with Different Dosages of $Ni(Ac)_2$

		$C_{Ni(Ac)2}$ (g/L)					
		0	1	5	10	15	20
(A) TiO_2	$a = b$	3.8040	3.7900	3.7967	3.8046	3.7897	3.7838
	c (nm)	9.7198	9.5878	9.6199	9.7127	9.5285	9.5349
	cell volume (nm^3)	140.65	137.72	138.67	140.59	136.85	136.51
(R) TiO_2	$a = b$	4.6329	4.6129	4.6435	4.636	4.6030	4.6094
	c (nm)	2.9692	2.9629	2.9518	2.9741	2.9549	2.9630
	cell volume (nm^3)	63.73	63.05	63.65	63.92	62.61	62.95

are at about 458.6, 464.4, 873.53, and 857.05 eV, respectively, demonstrating that the main chemical states of Ni and Ti in the samples are +2 and +4 valence, respectively. However, the intensity of XPS peak corresponding to $Ni_{2p}3/2$ is very weak, which means that the amount of Ni in the surface of the film is very small, which is consistent with the results of EDS analysis.

The O_{1s} XPS spectra are wide and asymmetric, indicating that there are at least two kinds of chemical states, including crystal lattice oxygen (O_L) and chemiadsorbed oxygen (O_H) with increasing binding energy. Thus, the O_{1s} XPS spectrum is fitted to two kinds of chemical states in terms of Gaussian rule, as shown in Figure 3c. The binding energy of O_L and O_H are 530.2 and 531.5 eV, respectively. The O_L XPS is mainly attributed to the contribution of Ti−O in TiO_2 crystal lattice, and the O_H XPS is closely related to the hydroxyl groups resulting mainly from the chemisorbed water, which are considered to favor photocatalytic reactions reported in many references (23). Interestingly, Figure 3c shows that the amount of O_H for the undoped sample is much less than that of O_L, whereas the amount of O_H in the Ni-doped sample is much more than that of O_L, demonstrating that the Ni doping enhances O_H content of TiO_2 greatly. And the increase in O_H content is liable to increase the hydrophilicity of TiO_2 film, which may be due to the synergy effect of the oxide containing Ni^{2+} with TiO_2.

3.4. DRS Spectrum of Film Catalysts. The UV−vis−DRS spectra of different TiO_2 film catalysts are shown in Figure 4. Compared with the undoped sample, DRS spectrum of doped samples gradually shifts to the red with increasing dosages and the absorption intensity also increases correspondingly. According to eq 1 (24), the band gap values can be evaluated from absorption spectra.

$$\alpha h\nu = A(h\nu - E_g)^{n/2} \quad (1)$$

where E_g is the optical energy band gap, $h\nu$ is photon energy, α is absorption coefficient, and A is the characteristic parameter for respective transitions, regardless of photon energy; n is equal to 1 for direct gap and 4 for indirect gap. The values of E_g for direct and indirect transitions can be obtained by the linear relation and the extrapolation method, with the results shown in Table 3. On the basis of the above deduction and the results shown in Figure 4b, both the direct and indirect transition band gaps of the TiO_2 films are deduced with the increase in dosage. This means that the band gap was narrowing after doping. Ni doped TiO_2 films enhances the light utilization of the film, which is related to the increase in the rutile and Ni dosage in the film.

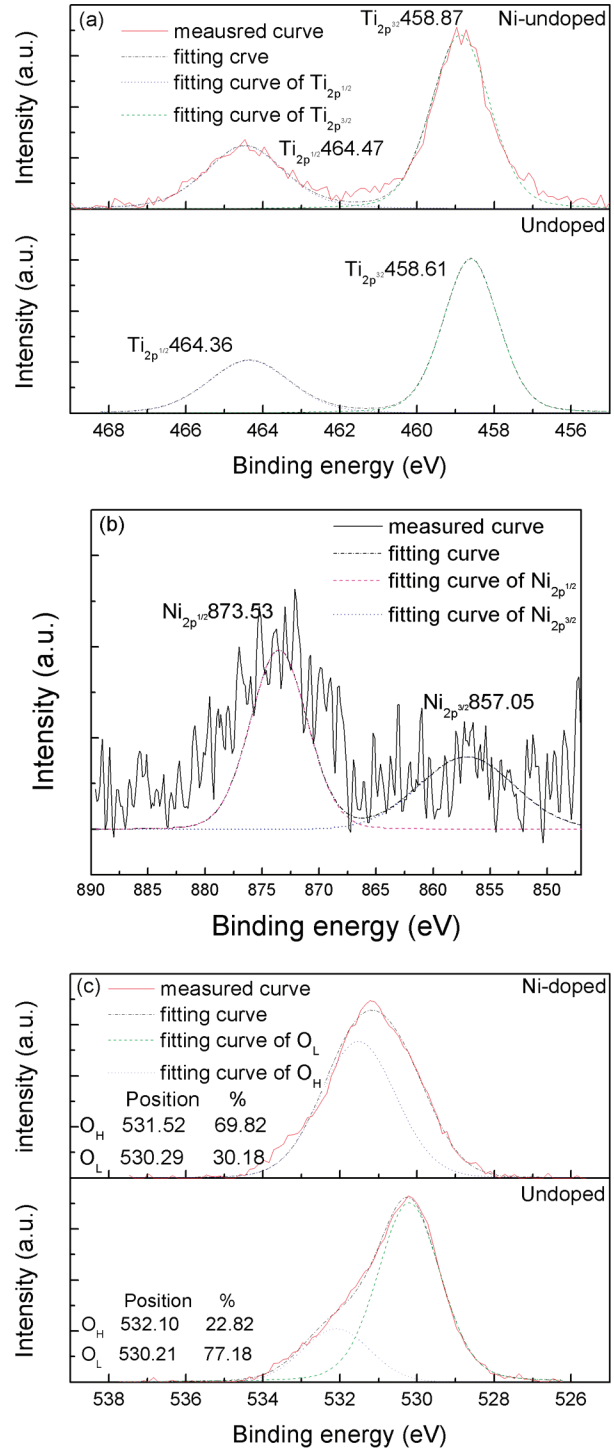

FIGURE 3. XPS analyses of film catalysts without and with doping of 10 g/L $Ni(Ac)_2$. (a) XPS spectrum of Ti_{2p}; (b) XPS spectrum of Ni_{2p}; (c) XPS of O_{1s}.

3.5. Photocatalytic Property of Film Catalysts. The photocatalytic activity of TiO_2 film catalysts was evaluated by photocatalytic splitting Na_2S+Na_2SO_3 solution into H_2. The rate of H_2 evolution is shown in Figure 5. The larger

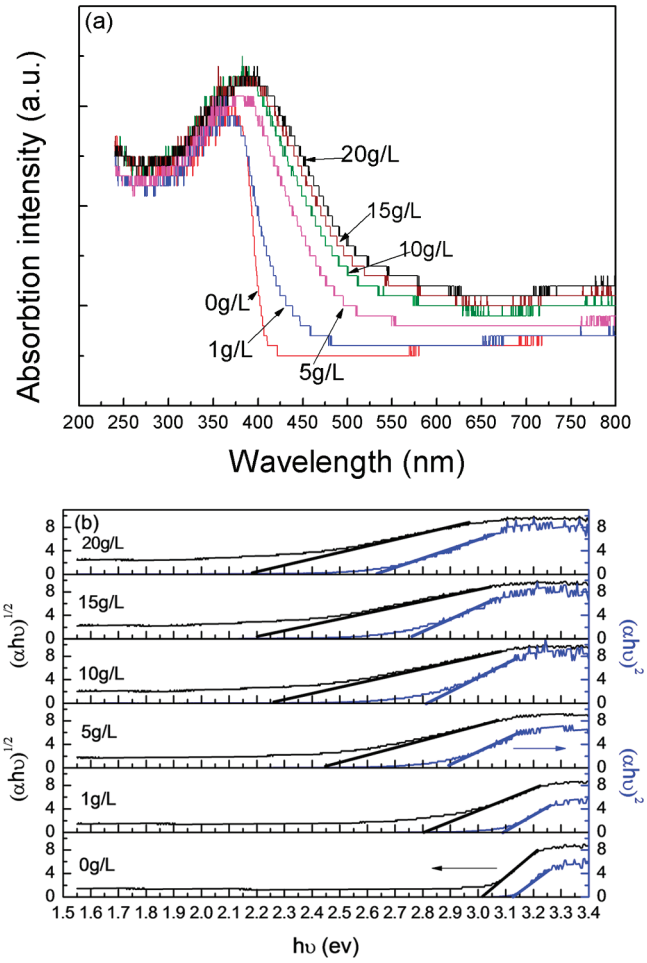

FIGURE 4. The optical absorption characters of film catalysts with different dosages. (a) UV−vis−DRS spectra of film catalysts; (b) direct and indirect transition band gaps of film catalysts.

Table 3. Values of E_g for Direct and Indirect Transitions of Film Catalysts Prepared with Different Dosages of $Ni(Ac)_2$

	$C_{Ni(Ac)2}$ (g/L)					
	0	1	5	10	15	20
E_g for direct transition (eV)	3.02	2.81	2.45	2.26	2.20	2.18
E_g for indirect transition(eV)	3.13	3.10	2.89	2.82	2.76	2.65

the rate of H_2 evolution is, the higher the photocatalytic reducing activity. As seen from Figure 5, among TiO_2 film catalysts, that doped with 10 g/L $Ni(AC)_2$ by the PEO process exhibits the highest photocatalytic reducing activity. Generally speaking, anatase has better photocatalytic activity than rutile; therefore, the decrease in the anatase will reduce the photocatalytic activity. On the other hand, the doping Ni changes the lattice structure of TiO_2 film and expands the optical absorption range, which is liable to improve the photocatalytic activity. The mutual effects of the two opposite changing trends leads to the best photocatalytic reducing activity obtained at the dosage of 10 g/L.

4. CONCLUSIONS

(1) Ni-doped TiO_2 film catalysts are composed of anatase and rutile TiO_2 with a microporous structure. The effects of

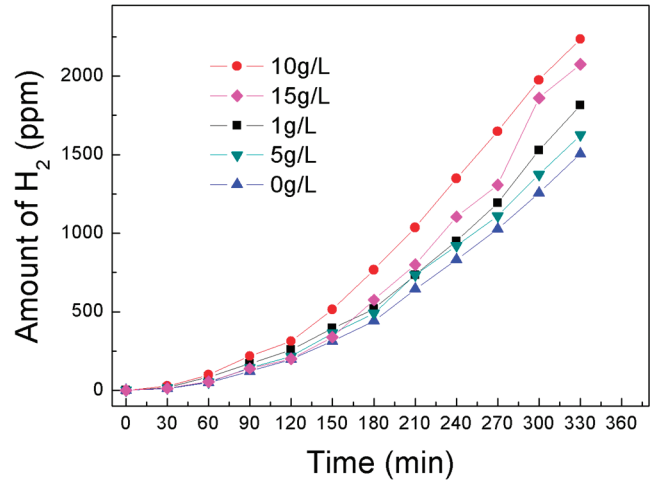

FIGURE 5. Amount of H_2 evolution in $Na_2S + Na_2SO_3$ solution by photocatalytic process of film catalysts.

Ni doping on the structure and phase composition of the film catalysts are related to the growth stress of the film and the radius and dosage of Ni^{2+}. (2) The optical absorption range of TiO_2 film gradually expands and shifts to the red with increasing dosages. Both the direct and indirect transition band gaps of the TiO_2 films are deduced consequently. Therefore, the light utilization of TiO_2 films is enhanced. (3) The photocatalytic activity of the film is related to the amount of the catalysts in the film and the optical absorption property, which determined that the best dosage $Ni(Ac)_2$ is 10 g/L in the preparation of film catalysts for the photocatalytic splitting $Na_2S+Na_2SO_3$ solution into H_2.

Acknowledgment. This work was financially supported by the National High Technology Research and Development Program of China (2007AA03Z337).

REFERENCES AND NOTES

(1) Chen, X. B.; Samuel, S. M. *Chem. Rev.* **2007**, *107*, 2891–2959.
(2) Gomathi, D. L.; Narasimha, M. B.; Girish, K. S. *J. Mol. Catal. A: Chem.* **2009**, *308*, 174–181.
(3) Dholam, R.; Patel, N.; Adami, M.; Miotello, A. *Int. J. Hydrogen Energy* **2009**, *34*, 5337–5346.
(4) Trenczek-Zajac, A.; Radecka, M.; Jasinski, M.; Michalow, K. A.; Rekas, M.; Kusior, E.; Zakrzewska, K.; Heel, A.; Graule, T.; Kowalski, K. *J. Power Sources* **2009**, *194*, 104–111.
(5) Wantala, K.; Tipayarom, D.; Laokiat, L.; Grisdanurak, N. *React. Kinet. Catal. Lett.* **2009**, *97*, 249–254.
(6) Das, K.; Sharma, S. N.; Kumar, M.; De, S. K. *J. Phys. Chem. C* **2009**, *113*, 14783–14792.
(7) Visinescu, C. M.; Sanjines, R.; Levy, F.; Parvulescu, V. I. *Appl. Catal., B* **2005**, *60*, 155–162.
(8) Gomathi, D. L.; Kottam, N.; Girish, K. S. *J. Phys. Chem. C* **2009**, *113*, 15593–15601.
(9) Lopez, R.; Gomez, R.; Llanos, M. E.*Catal. Today* **2009**, *148*, 103–108.
(10) Gomathi, D. L.; Narasimha, M. B.; Girish, K. S. *Mater. Sci. Eng., B* **2010**, *166*, 1–6.
(11) Begum, N. N. S.; Ahmed, H. M. F.; Gunashekar, K. R. *Bull. Mater. Sci.* **2008**, *31*, 747–751.
(12) Li, X. Z.; Liu, H. L.; Yue, P. T.; Sun, Y. P. *Environ. Sci. Technol.* **2000**, *34*, 4401–4406.
(13) Han, Y.; Chen, D. H.; Zhang, L. *Nanotechnology* **2008**, *19*, 335705.
(14) Wan, L.; Li, J. F.; Feng, J. Y.; Sun, W.; Ma, Z. Q. *Chin. J. Chem. Phys.* **2008**, *21*, 487–492.
(15) Yao, Z. P.; Jia, F. Z.; Jiang, Y. L.; Li, C. X.; Jiang, Z. H.; Bai, X. F. *Appl. Surf. Sci.* **2010**, *256*, 1793–1797.
(16) Bayati, M. R.; Moshfegh, A. Z.; Golestani-Fard, F. *Electrochim. Acta* **2010**, *55*, 3093–3102.

(17) Bayati, M. R.; Golestani-Fard, F.; Moshfegh, A. Z. *Appl. Surf. Sci.* **2010**, *256*, 4253–4259.
(18) Bayati, M. R.; Golestani-Fard, F.; Moshfegh, A. Z. *Mater. Chem. Phys.* **2010**, *120*, 582.
(19) Sreethawong, T.; Suzuki, Y.; Yoshikawa, S. *Int. J. Hydrogen Energy* **2005**, *30*, 1053–1062.
(20) Yu, H.; Li, X. J.; Zheng, S. J.; Xu, W. *Mater. Chem. Phys.* **2006**, *97*, 59.
(21) Begum, N. S.; Farveez Ahmed, H. M.; Gunashekar, K. R. *Bull. Mater. Sci.* **2008**, *31*, 747–751.
(22) Khan, R. H. U.; Yerokhin, A. L.; Pilkington, T.; Leyland, A.; Matthews, A. *Surf. Coat. Technol.* **2005**, *200*, 1580–1586.
(23) Jing, L. Q.; Xin, B. F.; Yuan, F. L.; Xue, L. P.; Wang, B. Q.; Fu, H. G. *J. Phys. Chem. B* **2006**, *110*, 17860–17865.
(24) Gujar, T. P.; Shinde, V. R.; Lokhande, C. D.; Maneb, R. S.; Han, S. H. *Appl. Surf. Sci.* **2005**, *250*, 161–167.

AM100450H